Inverted Sedimentation of Active Particles in Unbiased ac Fields

José Carlos Ureña Marcos and Benno Liebchen*
Institut für Physik Kondensierter Materie, Technische Universität Darmstadt, Hochschulstraße 8, 64289 Darmstadt, Germany

(Received 28 September 2022; accepted 26 June 2023; published 21 July 2023)

Gaining control over the motion of active particles is crucial for applications ranging from targeted cargo delivery to nanomedicine. While much progress has been made recently to control active motion based on external forces, flows, or gradients in concentration or light intensity, which all have a well-defined direction or bias, little is known about how to steer active particles in situations where no permanent bias can be realized. Here, we show that ac fields with a vanishing time average provide an alternative route to steering active particles. We exemplify this route for inertial active particles in a gravitational field, observing that a substantial fraction of them persistently travels in the upward direction upon switching on the ac field, resulting in an inverted sedimentation profile at the top wall of a confining container. Our results offer a generic control principle that could be used in the future to steer active motion, direct collective behaviors, and purify mixtures.

DOI: 10.1103/PhysRevLett.131.038201

Introduction.—Active particles (APs) use energy from their environment to create directed motion. Examples comprise living organisms [1–3], both macroscopic—like the birds which form a flock [4]—and microscopic—such as sperm cells [5] and motile bacteria [6], as well as synthetic APs, like motile robots [7,8], Janus colloids [9–15], and droplet swimmers [16–23].

While biological microswimmers can steer autonomously and use this ability to perform sophisticated tasks [24], including food search [25,26], target detection [27], and the coordination of their collective behavior through communication [28,29], synthetic APs rely on external control schemes if they are to perform tasks like targeted drug delivery [30], microsurgery [31], and microplastic collection [32] in the future. Thus, following the importance of externally steering active motion, a wide range of control schemes has been recently developed. In particular, it is now well known that APs can be controlled via external fields, such as electric fields [33], (rotating) magnetic fields [34–36], or light intensity gradients [37–43], as well as with combinations of electric and magnetic fields, which allow the APs to collect, transport, and release cargo at intended locations [44]. There are now also established ways to steer APs with topographical features in their environment [45–47], boundaries [48], and feedback-control systems [49–51], as well as with external stimuli (gradient fields) acting on the swimming direction of synthetic APs via tactic phenomena, including chemotaxis [52–54], phototaxis [55–58], gravitaxis [59,60], thermotaxis [61], or viscotaxis [62–64].

Notably, all these control schemes involve fields with a well-defined direction or bias, which may be stationary or vary slowly with time (in such a way that APs can follow them adiabatically). Conversely, fast and unbiased ac fields have so far been mainly used to endow particles with the ability to self-propel [65–71] or to collect cargo [44], but hardly to control the dynamics of APs.

Here, we show that rapidly oscillating ac fields provide a novel route to controlling the self-propulsion direction of APs without requiring any large-scale gradients, directed flows, forces, or torques. Instead, the control principle that we propose hinges on the stabilization of fixed points in the orientation dynamics of APs that would be unstable in the absence of ac fields. To exemplify this control principle, we consider APs sedimenting at the lower wall of a container. When switching on a rapidly oscillating ac field that couples to the orientation of the APs, we observe that most of the particles stop sedimenting and persistently self-propel in the upward direction, resulting in an inverted sedimentation profile at the top wall (Video S1 [72] and Fig. 1). This is achieved by exploiting (weak) inertial effects in APs to stabilize the fixed point corresponding to upward motion. In contrast to previous works [59,80], our control principle does not require gravitaxis (but is robust against both positive and negative gravitaxis), bottom heaviness, or nonspherical particle shapes. As we show, the control principle can also be applied to purify particle mixtures or to reverse transport. Detailed hydrodynamic simulations show that the control principle applies even to colloidal microswimmers for which inertia is commonly neglected.

Model.—To exemplify the idea of using ac fields to control self-propulsion, let us consider (inertial) active Brownian particles (ABPs) in two dimensions [12,81–83], self-propelling at a constant speed v_0 along the direction $\mathbf{n}(t) = (\cos\theta(t), \sin\theta(t))$, with θ being the orientation

angle of the particle with respect to the x axis. The particles are subjected to an external force $\mathbf{F}$ and a torque T, yielding the following equations of motion:

$$m\ddot{\mathbf{r}} + \gamma\dot{\mathbf{r}} = \gamma v_0 \mathbf{n} + \mathbf{F} + \gamma\sqrt{2D}\boldsymbol{\eta}, \tag{1}$$

$$J\ddot{\theta} + \gamma_r\dot{\theta} = T + \gamma_r\sqrt{2D_r}\eta_r, \tag{2}$$

where m and J are the mass and the moment of inertia of the particles; γ, γ_r, D, and D_r are, respectively, the translational and rotational damping (Stokes drag) and diffusion coefficients; and $\boldsymbol{\eta}(t)$ and $\eta_r(t)$ represent zero-mean, unit-variance Gaussian white noise. This model could be realized, e.g., based on autophoretic Janus colloids in a liquid, with light-powered Janus colloids in a gas, or with vibrated granulates.

Inverting sedimentation with ac fields.—As a first example, we consider particles in a gravitational field $\mathbf{F} = -mg\hat{e}_y$, where g is the effective gravitational constant, experiencing a torque $T = T(\theta, t) = I\cos\theta\sin(\omega t) - g_{bh}\cos\theta$, where the first term represents an ac field of frequency ω, strength I, and vanishing time average $\langle I\cos\theta\sin(\omega t)\rangle_t = 0$, which could be realized, e.g., with magnetic colloids [84–86], magnetotactic bacteria [87,88], or metallodielectric colloids [89] in time-dependent magnetic or electric fields, respectively, or with magnetized granular particles in ac magnetic fields [90] on (tilted) vibrating plates [8,91], as we further specify below. The second term represents an optional (downward) bias that can take a nonzero value, e.g., for bottom-heavy (bh) Janus particles [92–94] or shape-asymmetric vibrated granulates [8,59,91] on a tilted plate.

To reduce the parameter space, we now rescale space and time as $t^* = \gamma_r t/J$ and $\mathbf{r}^* = \gamma_r\mathbf{r}/(v_0 J)$, which simplifies Eqs. (1) and (2) to [note that $\boldsymbol{\eta}(t) = \sqrt{\gamma_r/J}\boldsymbol{\eta}(t^*)$] $m^*\ddot{\mathbf{r}}^* + \dot{\mathbf{r}}^* = \mathbf{n} - v_s^*\hat{e}_y + \sqrt{2D^*}\boldsymbol{\eta}$, $\ddot{\theta} + \dot{\theta} = [-g_{bh}^* + I^*\sin(\omega^* t^*)]\cos\theta + \sqrt{2D_r^*}\eta_r$, where overdots denote the derivative with respect to t^*. The dimensionless parameters $m^* = \gamma_r m/(J\gamma)$, $v_s^* = mg/(\gamma v_0)$, $D^* = \gamma_r D/(Jv_0^2)$, $g_{bh}^* = Jg_{bh}/\gamma_r^2$, and $D_r^* = JD_r/\gamma_r$ are fixed by the specific system under consideration, whereas $I^* = JI/\gamma_r^2$ and $\omega^* = J\omega/\gamma_r$ can be adjusted via the ac field, thus serving as our key control parameters. In what follows, we neglect translational inertia ($m^*\ddot{\mathbf{r}}^* = 0$), which is unimportant for our results.

We now perform Brownian dynamics simulations of ABPs, with and without rotational inertia, initialized at $\mathbf{r}_0^* = (x_0^*, y_0^*) = (0, 10)$ with uniformly distributed random orientations and vanishing angular velocities. We confine the particles between two horizontal walls placed at $y_b^* = 0$ and $y_t^* = 15$ by setting the vertical component of the particle velocity to zero if a particle moves toward either wall. The ac field is initially off ($I^* = 0$), and so the particles move downward due to the gravitational field [Figs. 1(a), 1(c), 1(e) and Video S1 [72]] both in the overdamped case ($J = 0$) and in the presence of inertia ($J > 0$). Once the ABPs have (almost) reached the stationary sedimentation profile [Figs. 1(d) and 1(f)] and their average position is close to the bottom wall [$\langle y^*\rangle \approx 0$, Fig. 1(a)], we switch on the ac field (at $t_{ac}^* = 50$). While overdamped particles simply continue sedimenting

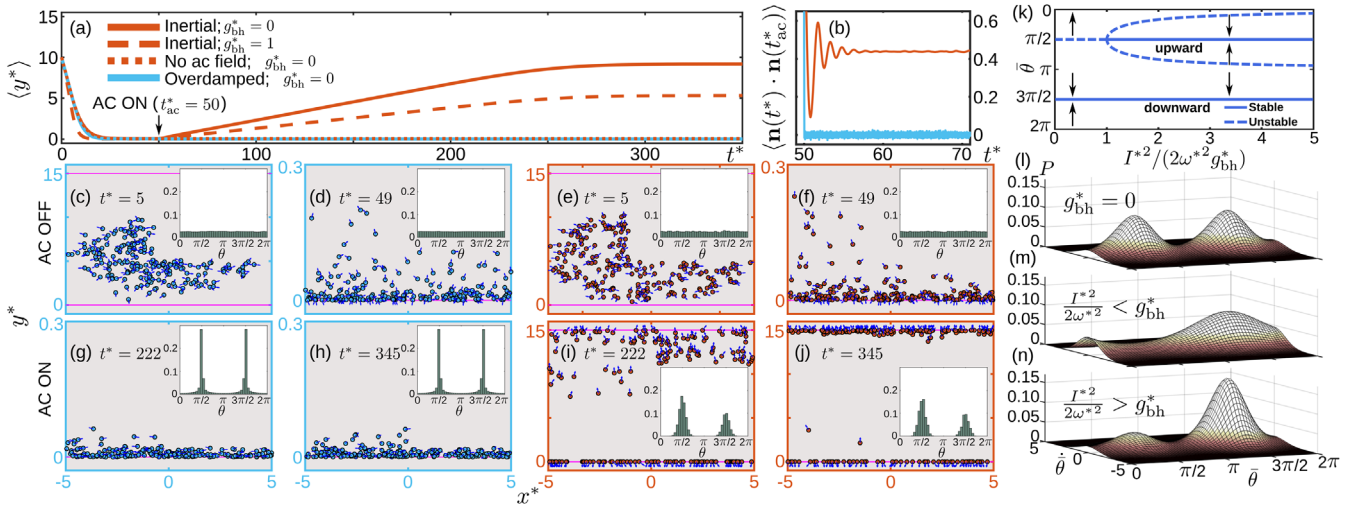

FIG. 1. (a) Average vertical position $\langle y^*\rangle$ of 10^4 inertial (red lines and frames) and rotationally overdamped (cyan) ABPs. (b) Autocorrelation of the self-propulsion direction after switching on the ac field. (c)–(j) Simulation snapshots of representative subsets of 200 ABPs with $g_{bh}^* = 0$. Dark blue arrows indicate self-propulsion direction. Insets: distribution of the self-propulsion directions over 20 oscillations of the ac field. Parameter values: $v_s^* = 0.9$, $D^* = 0.01$, $D_r^* = 1$, $I^{*2}/(2\omega^{*2}) = 0$ ($t^* < 50$), $I^{*2}/(2\omega^{*2}) = 20$ ($t^* \geq 50$), $\omega^* = 500$, time step $\Delta t^* = 10^{-4}/\omega^*$. (k) Bifurcation diagram corresponding to Eq. (3) with $D_r^* = 0$. Arrows indicate the flow of $\bar{\theta}$. The unstable fixed points for $I^{*2}/(2\omega^{*2}) > g_{bh}^*$ are given by $\bar{\theta} = -\arcsin(2\omega^{*2}g_{bh}^*/I^{*2}) + \pi$ and $\bar{\theta} = \arcsin(2\omega^{*2}g_{bh}^*/I^{*2})$. (l)–(n) $P(\bar{\theta}, \dot{\bar{\theta}})$ for $D_r^* = 1.5$ and (l) $g_{bh}^* = 0$, $I^{*2}/(2\omega^{*2}) = 5$, (m) $g_{bh}^* = 1$, $I^{*2}/(2\omega^{*2}) = 0.1$, (n) $g_{bh}^* = 1$, $I^{*2}/(2\omega^{*2}) = 5$.

[Figs. 1(g) and 1(h)], strikingly, in the presence of inertia, $\langle y^* \rangle$ suddenly starts increasing [Fig. 1(a)], until a plateau is reached at $\langle y^* \rangle > y_t^*/2$. That is, most of the inertial ABPs start to persistently move upward, against gravity, once the ac field is on [Fig. 1(i)]. This continues until they reach the top wall, resulting in an inverted sedimentation profile coexisting with a remaining (smaller) sedimentation profile at the bottom wall [Fig. 1(j)]. Remarkably, both profiles are exponential [80,95–97], with the one at the top wall showing a sedimentation length almost 2 orders of magnitude greater than that at the bottom wall for the chosen parameters (Fig. S1 in the Supplemental Material [72]). Note that the plateau value of $\langle y^* \rangle$ depends not only on the choice of parameters but also on the initial sign of I^* (Fig. S2 in the Supplemental Material [72]). However, at late times, fluctuations induce random flips between up- and downward motion (see Video S1 [72]), which leads to a slow decay of $\langle y^* \rangle$ to $y_t^*/2$ after $t^* \sim 10^4$ (not shown).

ac fields induce persistent orientation.—To understand the observed sedimentation reversal, let us now analyze the distribution of particle orientations. Before switching on the ac field, this distribution is uniform [insets in Figs. 1(c)–1(f)]. Upon switching on the field, overdamped particles essentially follow the (rapid) oscillations of the ac field, so that they self-propel about half of the time up- and downward [insets in Figs. 1(g) and 1(h)]. Thus, their net motion is essentially determined by the competition between the gravitational drift and translational diffusion, so the ac field hardly impacts the sedimentation profile. In stark contrast, for inertial APs, the ac field not only creates a significant upward bias [insets in Figs. 1(i) and 1(j)], but also stabilizes the particle orientation, as shown by its autocorrelation function in Fig. 1(b). This allows them to persistently self-propel toward the top wall (see Video S1 [72]).

Why do ac fields reverse the sedimentation profile?—To understand the bias and the persistence observed in the particle orientations, we now decompose θ into a "fast" component θ_{ac}, which is expected to oscillate on the same timescale as the ac field, and a "slow" part $\bar{\theta}$ representing the net dynamics after averaging over the ac field; i.e., $\theta = \bar{\theta} + \theta_{ac}$. Plugging $\theta = \bar{\theta} + \theta_{ac}$ into the equations of motion and averaging over the period of the ac field, we obtain (see the Supplemental Material [72])

$$\ddot{\bar{\theta}} + \dot{\bar{\theta}} = -\partial_{\bar{\theta}} U^*_{\mathrm{eff}}(\bar{\theta}) + \sqrt{2D_r^*}\eta_r, \tag{3}$$

$$U^*_{\mathrm{eff}}(\bar{\theta}) = g^*_{\mathrm{bh}} \sin\bar{\theta} + \frac{I^{*2}}{4\omega^{*2}} \cos^2\bar{\theta}. \tag{4}$$

Note that it is sufficient to explore the orientation dynamics of the particles, which is not influenced by their spatial dynamics.

It is instructive to first discuss the case of vanishing noise ($D_r^* = 0$). Equations (3) and (4) show that $\bar{\theta}_{up} = \pi/2$ and $\bar{\theta}_{down} = 3\pi/2$ are always fixed points. Performing a linear stability analysis of Eq. (3) shows that $\bar{\theta}_{down}$ is always stable, whereas $\bar{\theta}_{up}$ is stable only if $I^{*2}/(2\omega^{*2}) > g^*_{bh}$, a result resembling dynamical stabilization [98–102]. This condition leads to a subcritical pitchfork bifurcation, with both fixed points being stable and their basins of attraction equally large for $g^*_{bh} = 0$ and $|I^*| > 0$ [Fig. 1(k)].

To understand the role of noise, we now consider the Fokker-Planck equation equivalent to Eqs. (3) and (4) [103], which yields the exact steady-state probability distributions $P(\bar{\theta}, \dot{\bar{\theta}}) = N \exp\{-\alpha[\dot{\bar{\theta}}^2 + 2U^*_{\mathrm{eff}}(\bar{\theta})]\}$ and

$$P(\bar{\theta}) = N_{\bar{\theta}} \exp\left[-\frac{1}{D_r^*} U^*_{\mathrm{eff}}(\bar{\theta})\right], \tag{5}$$

where $\alpha = (2D_r^*)^{-1}$, $N = (1/\sqrt{2\pi D_r^*})\{\int_0^{2\pi} \exp[-(1/D_r^*) U^*_{\mathrm{eff}}(\bar{\theta})] d\bar{\theta}\}^{-1}$, and $N_{\bar{\theta}} = \sqrt{2\pi D_r^*} N$ (details in the Supplemental Material [72]). Equation (5) is essentially a Boltzmann distribution for the slow variable $\bar{\theta}$ in the effective potential U^*_{eff}. The maxima of $P(\bar{\theta}, \dot{\bar{\theta}})$ and $P(\bar{\theta})$ coincide with the stable equilibrium points encountered for the noiseless case, and we recover the condition $I^{*2}/(2\omega^{*2}) > g^*_{bh}$ for stabilizing the upper fixed point, as illustrated in Figs. 1(l)–1(n). Importantly, however, rotational diffusion strongly affects the relative probability of the maxima as it broadens the peaks in Figs. 1(l)–1(n) and tends to even them out. This analytical result sheds light on the phenomenon of inverted sedimentation: if $I^{*2}/(2\omega^{*2}) > g^*_{bh}$ (in physical units $I^2 > 2J\omega^2 g_{bh}$) is fulfilled, and $\omega^* \gg \sqrt{g^*_{bh}}, \sqrt{I^*}$ (or $\omega \gg \sqrt{g_{bh}/J}, \sqrt{I/J}$) for Eqs. (3) and (4) to be meaningful (see Fig. 2), the ac field stabilizes upward self-propulsion, and thus the ABPs that happen to be pointing upward the moment the ac field is switched on persistently travel toward the top wall, in competition with fluctuations.

Delay effects.—Let us now provide an explanation of the physical mechanism allowing the ac field to stabilize the upper fixed point. Whereas the orientation of overdamped ABPs essentially follows the oscillations of the ac field, inertial ABPs show a delay in their response to the field [104] [Fig. 1(b)]. Thus, during each oscillation, there are time instants when the particle orientation turns away from the vertical direction, while the ac field pushes it toward the fixed point. The inverse process, where the particle orientation turns into the vertical position while the ac field pushes it away from the fixed point, is less efficient, since the torque resulting from the ac field is weaker close to the fixed point. That is, (tiny) delay effects are crucial to observe inverted sedimentation. For $g_{bh} = 0$, the minimum strength of inertia is determined by the condition $\omega \gg \sqrt{I/J}$; that is, the frequency of the ac field must be high enough for the particles to be unable to closely follow it, due to inertia.

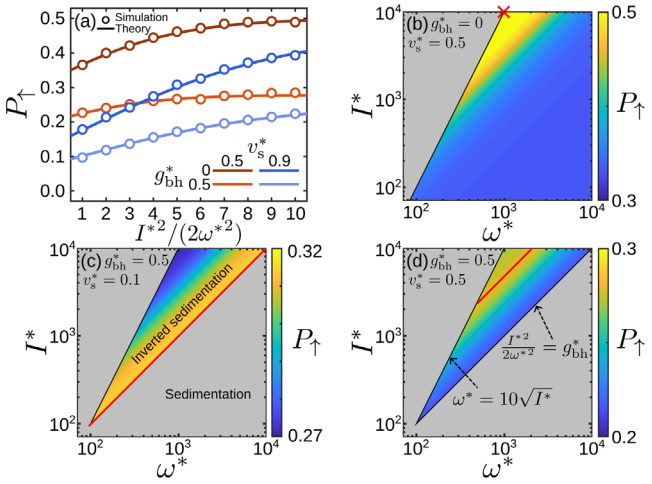

FIG. 2. (a) $P_\uparrow$ as a function of $I^{*2}/(2\omega^{*2})$ obtained from Eqs. (5) and (6) (solid lines) and simulations of 10^4 ABPs (dots), where we calculate $P_\uparrow$ as the fraction of particles with $\sin(\theta) > v_s^*$ at the end of the simulation ($t^* = 400$). (b)–(d) $P_\uparrow$ obtained from Eqs. (5) and (6). Gray and colored regions show normal and inverted sedimentation, respectively, where we define the transition line as $I^{*2} = 2g^*_{\rm bh}\omega^{*2}$ and $\omega^* = 10\sqrt{I^*}$ [for $I^* > g^*_{\rm bh}$; Eq. (7)]. The maximum of $P_\uparrow$ is marked in red. Parameters: $D^* = 0.01$, $D^*_r = 1$, $\omega^* = 500$, simulation time step $\Delta t^* = 10^{-2}/\omega^*$, $t^*_{\rm ac} = 50$.

What controls the fraction of particles moving upward?—Particles move upward if the vertical component of their self-propulsion velocity exceeds the gravitational drift, i.e., if $v_0 \sin\theta > mg/\gamma$, which leads to a steady-state probability

$$P_\uparrow = P[\sin(\bar{\theta}) > v_s^*] = \int_{\arcsin(v_s^*)}^{\pi-\arcsin(v_s^*)} P(\bar{\theta})d\bar{\theta}. \quad (6)$$

By numerically evaluating this integral, we can predict the full parameter dependence of the fraction of particles sedimenting at the top (Fig. 2) in close quantitative agreement with our simulations [Fig. 2(a)]. Note that, for the comparison with the analytical results, in the simulations we average $P_\uparrow$ over the $I^* < 0$ and $I^* > 0$ cases to achieve faster convergence of our results (see the Supplemental Material [72]). As expected, $P_\uparrow$ broadly decreases with increasing bottom heaviness ($g^*_{\rm bh}$) and sedimentation speed (v^*_s). Strikingly, however, the dependence of $P_\uparrow$ on I^* and ω^* is highly nontrivial and nonmonotonic, as shown in Figs. 2(b)–2(d) and Fig. S5 in the Supplemental Material [72], where red lines and crosses indicate the maximum of $P_\uparrow$. Importantly, inverted sedimentation typically sets in with a finite probability $P_\uparrow$ (as typical for subcritical transitions) exceeding 20% in most cases.

Parameters: How much inertia is needed?—The two criteria to observe inverted sedimentation read (in dimensional units)

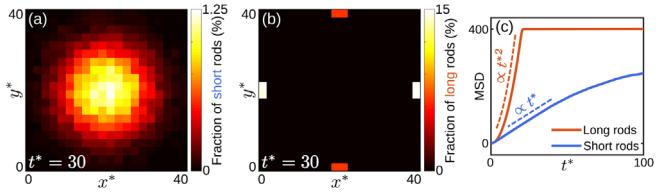

FIG. 3. (a),(b) Spatial distribution of 2×10^4 (a) short and (b) long rod-shaped ABPs under the application of an ac pressure field and (c) their mean square displacement (MSD). Long rods are 5 times longer than short rods. Details can be found in the Supplemental Material [72].

$$\omega \gg \sqrt{g_{\rm bh}/J}, \sqrt{I/J} \quad \text{and} \quad I^2 > 2J\omega^2 g_{\rm bh}. \quad (7)$$

These expressions reflect that our control scheme requires inertia, but fails if J is too large. How much inertia is needed depends on the system under investigation and the driving frequency. As an example, let us consider magnetic Janus colloids of radius $R = 2$ μm [105] in a liquid, where inertia is typically neglected. Even if the particles are bottom heavy ($g_{\rm bh} \sim m_{\rm cap} gR/2$ [80]) and experience a downward bias, for a cap of mass $m_{\rm cap} \sim 10^{-15}$ kg [105], upward self-propulsion can be stabilized with a magnetic field of frequency $\sim 10^4$ Hz exerting a torque $I \sim 10^{-17}$ N m on the colloids [105], corresponding to 0.01 mT. Slower drivings are required when using magnetized vibrated granulates [90] on tilted plates [8,91] in an ac magnetic field, where inertial effects are substantially stronger (details in the Supplemental Material [72]).

Inverted transport.—To demonstrate the generality of our control principle, we show in Fig. S7 and Video S2 in the Supplemental Material [72] that rapidly oscillating ac fields can be used to reverse the direction of motion of APs in a periodic light intensity field.

ac pressure fields.—Notably, the proposed control scheme also applies to particles whose orientation does not couple to electric, magnetic, or light fields. When applying an ac pressure field (sound wave) with a suitable frequency and intensity to rod-shaped active particles, we find that short rods exhibit active diffusion [Figs. 3(a) and 3(c)] [82,83], whereas the orientation of longer rods is stabilized by the ac field. Consequently, only the longer rods move persistently [Figs. 3(b) and 3(c)], and so the ac control scheme allows for the sorting of elongated active particles by length (details in the Supplemental Material [72]).

Hydrodynamics and autophoresis.—To show that our results apply to actual Janus colloids at the microscale, finally, we perform detailed finite element simulations of an autophoretic Janus colloid in an ac field for realistic parameters, e.g., for Janus colloids with a magnetic dipole moment [105] in an ac magnetic field (details in the Supplemental Material [72]). We explicitly solve for the coupled dynamics of the phoretic field, the solvent flow

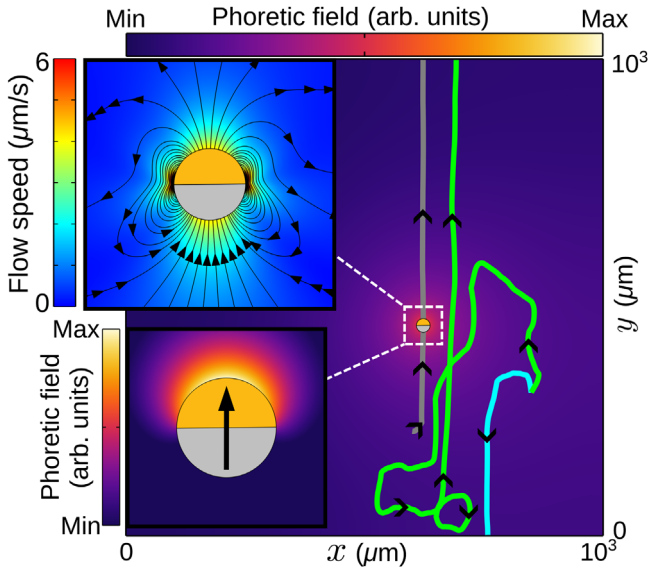

FIG. 4. Exemplary trajectories of Janus colloids in an unbiased ac field showing sedimentation (cyan) and inverted sedimentation (gray and green). The background represents the phoretic field created by the colloid corresponding to the gray trajectory, which is depicted 15 times its actual size. Insets: flow (top) and phoretic (bottom) fields close to the colloid, with arrows indicating the flow direction (top) and the instantaneous direction of motion of the Janus colloid (bottom). Details in the Supplemental Material [72].

field, and the dynamics of the Janus particle. These simulations account for the full hydrodynamic (and phoretic) interactions with the surrounding walls and predict stable upward (and downward) motion at late times (Fig. 4 and Videos S3 and S4 [72]).

Conclusions.—Our results unveil a generic principle to control the motion of APs by stabilizing fixed points in their orientation dynamics with ac fields. Unlike other schemes for controlling self-propulsion, this scheme does not require an explicit bias, but works even for external fields with a vanishing time average. This offers several advantages: (i) All particles are identically controlled, as opposed to, e.g., particles that are placed at different positions in a rotating flow field or in a rotating magnetic field. (ii) There is no need to realize any large-scale gradients as required, e.g., for tactic mechanisms. Accordingly, control can be readily switched on and off, which is not easily possible for mechanisms like chemotaxis or thermotaxis, where a complete renewal of the underlying concentration or temperature field would be required. (iii) The mechanism works even for particles with isotropic shape, as opposed to, e.g., viscotaxis [62] or gravitaxis [59], and without internal asymmetries in their mass distribution [92]. (iv) The mechanism is generic. It can be applied to, e.g., active rods in ac pressure fields, phototactic Janus colloids, active colloids featuring a permanent electric or magnetic dipole moment, or vibrated granular particles. Possible applications include the inversion of sedimentation profiles, transport reversal, the purification of ensembles of Janus colloids, and the sorting of active rods. In the future, the same control scheme could also be used to direct the collective behavior of APs or to segregate particle ensembles by inertia, size, or coating geometry.

*benno.liebchen@pkm.tu-darmstadt.de

[1] M. C. Marchetti, J. F. Joanny, S. Ramaswamy, T. B. Liverpool, J. Prost, M. Rao, and R. A. Simha, Rev. Mod. Phys. **85**, 1143 (2013).
[2] D. Klotsa, Soft Matter **15**, 8946 (2019).
[3] W. Nachtigall, Math. Meth. Appl. Sci. **24**, 1401 (2001).
[4] A. Cavagna and I. Giardina, Annu. Rev. Condens. Matter Phys. **5**, 183 (2014).
[5] S. Rode, J. Elgeti, and G. Gompper, New J. Phys. **21**, 013016 (2019).
[6] A. Be'er and G. Ariel, Mov. Ecol. **7**, 9 (2019).
[7] M. Mijalkov, A. McDaniel, J. Wehr, and G. Volpe, Phys. Rev. X **6**, 011008 (2016).
[8] C. Scholz, M. Engel, and T. Pöschel, Nat. Commun. **9**, 931 (2018).
[9] J. Zhang, B. A. Grzybowski, and S. Granick, Langmuir **33**, 6964 (2017).
[10] W. Paxton, K. Kistler, C. Olmeda, A. Sen, S. St. Angelo, Y. Cao, T. Mallouk, P. Lammert, and V. Crespi, J. Am. Chem. Soc. **126**, 13424 (2004).
[11] J. R. Howse, R. A. L. Jones, A. J. Ryan, T. Gough, R. Vafabakhsh, and R. Golestanian, Phys. Rev. Lett. **99**, 048102 (2007).
[12] C. Bechinger, R. Di Leonardo, H. Löwen, C. Reichhardt, G. Volpe, and G. Volpe, Rev. Mod. Phys. **88**, 045006 (2016).
[13] Y. Shelke, N. R. Srinivasan, S. P. Thampi, and E. Mani, Langmuir **35**, 4718 (2019).
[14] B. Liebchen and A. K. Mukhopadhyay, J. Phys. Condens. Matter **34**, 083002 (2021).
[15] H. R. Vutukuri, M. Hoore, C. Abaurrea-Velasco, L. van Buren, A. Dutto, T. Auth, D. A. Fedosov, G. Gompper, and J. Vermant, Nature (London) **586**, 52 (2020).
[16] Z. Izri, M. N. van der Linden, S. Michelin, and O. Dauchot, Phys. Rev. Lett. **113**, 248302 (2014).
[17] N. Cira, A. Benusiglio, and M. Prakash, Nature (London) **519**, 446 (2015).
[18] C. Krüger, G. Klös, C. Bahr, and C. C. Maass, Phys. Rev. Lett. **117**, 048003 (2016).
[19] L. Wang, B. Yuan, J. Lu, S. Tan, F. Liu, L. Yu, Z. He, and J. Liu, Adv. Mater. **28**, 4065 (2016).
[20] C. Jin, B. V. Hokmabad, K. A. Baldwin, and C. C. Maass, J. Phys. Condens. Matter **30**, 054003 (2018).
[21] B. V. Hokmabad, R. Dey, M. Jalaal, D. Mohanty, M. Almukambetova, K. A. Baldwin, D. Lohse, and C. C. Maass, Phys. Rev. X **11**, 011043 (2021).
[22] S. Suda, T. Suda, T. Ohmura, and M. Ichikawa, Phys. Rev. Lett. **127**, 088005 (2021).

[23] D. Cholakova, M. Lisicki, S. Smoukov, S. Tcholakova, E. Lin, J. Chen, G. Canio, E. Lauga, and N. Denkov, Nat. Phys. **17**, 1050 (2021).
[24] J. Elgeti, R. G. Winkler, and G. Gompper, Rep. Prog. Phys. **78**, 056601 (2015).
[25] V. Sourjik and N. S. Wingreen, Curr. Opin. Cell Biol. **24**, 262 (2012).
[26] J. Cremer, T. Honda, Y. Tang, J. Wong-Ng, M. Vergassola, and T. Hwa, Nature (London) **575**, 658 (2019).
[27] L. Alvarez, B. M. Friedrich, G. Gompper, and U. B. Kaupp, Trends Cell Biol. **24**, 198 (2014).
[28] J. Noorbakhsh, D. J. Schwab, A. E. Sgro, T. Gregor, and P. Mehta, Phys. Rev. E **91**, 062711 (2015).
[29] Z. Eidi, F. Mohammad-Rafiee, M. Khorrami, and A. Gholami, Soft Matter **13**, 8209 (2017).
[30] A. Ghosh, W. Xu, N. Gupta, and D. H. Gracias, Nano Today **31**, 100836 (2020).
[31] J. Vyskočil, C. Mayorga-Martinez, E. Jablonska, F. Novotný, T. Ruml, and M. Pumera, ACS Nano **14**, 8247 (2020).
[32] L. Wang, A. Käppler, D. Fischer, and J. Simmchen, ACS Appl. Mater. Interfaces **11**, 32937 (2019).
[33] B. Zhang, A. Snezhko, and A. Sokolov, Phys. Rev. Lett. **128**, 018004 (2022).
[34] J. Palacci, S. Sacanna, A. Vatchinsky, P. M. Chaikin, and D. J. Pine, J. Am. Chem. Soc. **135**, 15978 (2013).
[35] M. Driscoll, B. Delmotte, M. Youssef, S. Sacanna, A. Donev, and P. Chaikin, Nat. Phys. **13**, 375 (2017).
[36] F. Martinez-Pedrero, H. Massana-Cid, and P. Tierno, Small **13**, 1603449 (2017).
[37] S. Nedev, S. Carretero-Palacios, P. Kühler, T. Lohmüller, A. S. Urban, L. J. E. Anderson, and J. Feldmann, ACS Photonics **2**, 491 (2015).
[38] Y. Zong, J. Liu, R. Liu, H. Guo, M. Yang, Z. Li, and K. Chen, ACS Nano **9**, 10844 (2015).
[39] H. Moyses, J. Palacci, S. Sacanna, and D. G. Grier, Soft Matter **12**, 6357 (2016).
[40] J. Liu, H.-L. Guo, and Z.-Y. Li, Nanoscale **8**, 19894 (2016).
[41] J. Liu and Z. Li, Micromachines **9**, 232 (2018).
[42] S. M. Mousavi, I. Kasianiuk, D. Kasyanyuk, S. K. P. Velu, A. Callegari, L. Biancofiore, and G. Volpe, Soft Matter **15**, 5748 (2019).
[43] I. Buttinoni, L. Caprini, L. Alvarez, F. J. Schwarzendahl, and H. Löwen, Europhys. Lett. **140**, 27001 (2022).
[44] A. F. Demirörs, M. T. Akan, E. Poloni, and A. R. Studart, Soft Matter **14**, 4741 (2018).
[45] J. Simmchen, J. Katuri, W. Uspal, M. Popescu, M. Tasinkevych, and S. Sanchez, Nat. Commun. **7**, 10598 (2016).
[46] J.-C. Wu, K. Lv, W.-W. Zhao, and B.-Q. Ai, Chaos **28**, 123102 (2018).
[47] M. Wang, Phys. Rev. E **103**, 042609 (2021).
[48] S. Das, A. Garg, A. Campbell, J. Howse, A. Sen, D. Velegol, R. Golestanian, and S. Ebbens, Nat. Commun. **6**, 8999 (2015).
[49] U. Khadka, V. Holubec, H. Yang, and F. Cichos, Nat. Commun. **9**, 3864 (2018).
[50] M. Fernández-Rodríguez, F. Grillo, L. Alvarez, M. Rathlef, I. Buttinoni, G. Volpe, and L. Isa, Nat. Commun. **11**, 4223 (2020).
[51] F. A. Lavergne, H. Wendehenne, T. Bäuerle, and C. Bechinger, Science **364**, 70 (2019).
[52] Y. Hong, N. M. K. Blackman, N. D. Kopp, A. Sen, and D. Velegol, Phys. Rev. Lett. **99**, 178103 (2007).
[53] B. Liebchen and H. Löwen, Acc. Chem. Res. **51**, 2982 (2018).
[54] N. Möller, S. Seiffert, T. Palberg, and R. Niu, ChemNanoMat **7**, 1145 (2021).
[55] C. Lozano, B. ten Hagen, H. Löwen, and C. Bechinger, Nat. Commun. **7**, 12828 (2016).
[56] J. R. Gomez-Solano, S. Samin, C. Lozano, P. Ruedas-Batuecas, R. van Roij, and C. Bechinger, Sci. Rep. **7**, 14891 (2017).
[57] C. Lozano, B. Liebchen, B. ten Hagen, C. Bechinger, and H. Löwen, Soft Matter **15**, 5185 (2019).
[58] S. Jahanshahi, C. Lozano, B. Liebchen, H. Löwen, and C. Bechinger, Commun. Phys. **3**, 127 (2020).
[59] B. ten Hagen, F. Kümmel, R. Wittkowski, D. Takagi, H. Löwen, and C. Bechinger, Nat. Commun. **5**, 4829 (2014).
[60] F. Rühle, A. Zantop, and H. Stark, Eur. Phys. J. E **45**, 26 (2022).
[61] S. Auschra, A. Bregulla, K. Kroy, and F. Cichos, Eur. Phys. J. E **44**, 90 (2021).
[62] B. Liebchen, P. Monderkamp, B. ten Hagen, and H. Löwen, Phys. Rev. Lett. **120**, 208002 (2018).
[63] C. Datt and G. J. Elfring, Phys. Rev. Lett. **123**, 158006 (2019).
[64] M. Stehnach, N. Waisbord, D. Walkama, and J. Guasto, Nat. Phys. **17**, 926 (2021).
[65] J. Chen, H. Zhang, X. Zheng, and H. Cui, AIP Adv. **4**, 31325 (2014).
[66] C. W. Shields and O. D. Velev, Chem **3**, 539 (2017).
[67] T. Mano, J.-B. Delfau, J. Iwasawa, and M. Sano, Proc. Natl. Acad. Sci. U.S.A. **114**, E2580 (2017).
[68] F. Nadal and S. Michelin, J. Fluid Mech. **898**, A10 (2020).
[69] Y. Wu, A. Fu, and G. Yossifon, Sci. Adv. **6**, eaay4412 (2020).
[70] J. G. Lee, A. Al Harraq, K. J. M. Bishop, and B. Bharti, J. Phys. Chem. B **125**, 4232 (2021).
[71] D. Nishiguchi, J. Iwasawa, H. R. Jiang, and M. Sano, New J. Phys. **20**, 015002 (2018).
[72] See Supplemental Material at http://link.aps.org/supplemental/10.1103/PhysRevLett.131.038201 for further details of inverted sedimentation, a detailed derivation of Eqs. (3) and (4), and a detailed discussion of rod segregation, inverted transport, and the finite element simulations, which includes Refs. [73–79].
[73] A. P. Solon, M. E. Cates, and J. Tailleur, Eur. Phys. J. Spec. Top. **224**, 1231 (2015).
[74] F. Ginot, A. Solon, Y. Kafri, C. Ybert, J. Tailleur, and C. Cottin-Bizonne, New J. Phys. **20**, 115001 (2018).
[75] B. D. Cullity and C. D. Graham, *Introduction to Magnetic Materials* (John Wiley & Sons, New York, 2008).
[76] J. Friend and L. Y. Yeo, Rev. Mod. Phys. **83**, 647 (2011).
[77] B. Liebchen and H. Löwen, J. Chem. Phys. **150**, 061102 (2019).
[78] J. L. Anderson, Annu. Rev. Fluid Mech. **21**, 61 (1989).
[79] T. Bickel, G. Zecua, and A. Würger, Phys. Rev. E **89**, 050303(R) (2014).

[80] K. Wolff, A. M. Hahn, and H. Stark, Eur. Phys. J. E **36**, 43 (2013).
[81] B. ten Hagen, S. Van Teeffelen, and H. Löwen, J. Phys. Condens. Matter **23**, 194119 (2011).
[82] H. Löwen, J. Chem. Phys. **152**, 040901 (2020).
[83] L. Hecht, J. C. Ureña, and B. Liebchen, arXiv:2102.13007.
[84] J. Palacci, S. Sacanna, A. P. Steinberg, D. J. Pine, and P. M. Chaikin, Science **339**, 936 (2013).
[85] K. Han and A. Snezhko, Lab Chip **21**, 215 (2021).
[86] Y. Li, S. Wang, X. Zhang, and Y. Gao, JCIS Open **8**, 100061 (2022).
[87] C. J. Pierce, E. Mumper, E. E. Brown, J. T. Brangham, B. H. Lower, S. K. Lower, F. Y. Yang, and R. Sooryakumar, Phys. Rev. E **95**, 062612 (2017).
[88] A. Petroff, A. Rosselli-Calderon, B. Roque, and P. Kumar, Phys. Rev. Fluids **7**, 053102 (2022).
[89] B. Behdani, K. Wang, and C. A. Silvera Batista, Soft Matter **17**, 9410 (2021).
[90] M. Ledesma-Motolinía, J. L. Carrillo-Estrada, A. Escobar, F. Donado, and P. Castro-Villarreal, Phys. Rev. E **107**, 024902 (2023).
[91] C. Scholz, S. Jahanshahi, A. Ldov, and H. Löwen, Nat. Commun. **9**, 5156 (2018).
[92] A. I. Campbell and S. J. Ebbens, Langmuir **29**, 14066 (2013).
[93] D. P. Singh, W. E. Uspal, M. N. Popescu, L. G. Wilson, and P. Fischer, Adv. Funct. Mater. **28**, 1706660 (2018).
[94] A. Rashidi, S. Razavi, and C. L. Wirth, Phys. Rev. E **101**, 042606 (2020).
[95] J. Palacci, C. Cottin-Bizonne, C. Ybert, and L. Bocquet, Phys. Rev. Lett. **105**, 088304 (2010).
[96] M. Enculescu and H. Stark, Phys. Rev. Lett. **107**, 058301 (2011).
[97] A. Scagliarini and I. Pagonabarraga, Soft Matter **18**, 2407 (2022).
[98] L. D. Landau and E. M. Lifshitz, *Mechanics* (Pergamon, Oxford, 1960).
[99] A. Stephenson, London, Edinburgh, Dublin Philos. Mag. J. Sci. **15**, 233 (1908).
[100] Y. B. Simons and B. Meerson, Phys. Rev. E **80**, 042102 (2009).
[101] E. I. Butikov, J. Phys. A **44**, 295202 (2011).
[102] W. Morzuch, Vib. Phys. Syst. **25**, 293 (2012), https://vibsys.put.poznan.pl/_journal/2012-25/2012-book.pdf.
[103] H. Risken, *The Fokker-Planck Equation* (Springer, Berlin, 1996).
[104] L. Caprini, R. K. Gupta, and H. Löwen, arXiv:2206.14324.
[105] S. K. Smoukov, S. Gangwal, M. Marquez, and O. D. Velev, Soft Matter **5**, 1285 (2009).